# Polarization model study of isotope effects in the gas phase hydronium–hydroxide neutralization reaction

Frank H. Stillinger and Thomas A. Weber

*Bell Laboratories, Murray Hill, New Jersey 07974*
(Received 7 December 1981; accepted 29 December 1981)

Using the polarization model to represent all interactions present, classical dynamical trajectories have been numerically generated for reactive collisions between hydronium and hydroxide ions. The four isotopic variants have been examined that are possible with reactants $H_3O^+$, $D_3O^+$, $OH^-$, and $OD^-$; 100 trajectories were created for each case. The results show a marked tendency for energy released by the neutralization to be concentrated on that water molecule whose oxygen originated in the hydroxide anion. Significant isotope effects appear in the various product distributions, the primary determinant of which is the mass of the transferred hydrogenic particle. These effects appear to stem from differences between the respective lifetimes of the reaction complexes.

## I. INTRODUCTION

The polarization model[1] was originally devised to represent interactions in the condensed phases of water, under circumstances where the ionic dissociation process was important:

$$H_2O \rightleftharpoons H^+ + OH^- \ . \tag{1.1}$$

However the generality of this model also confers upon it an immediate relevance to certain gas-phase processes such as ion hydration dynamics,[2] and the neutralization reaction occurring between acid–base cluster pairs.

In a previous publication[3] we have studied one of the simplest of the gas-phase neutralization reactions, namely that involving the hydronium cation and the hydroxide anion:

$$H_3O^+ + OH^- \rightarrow H_2O + H_2O \ . \tag{1.2}$$

The polarization model supplied the potential energy function over the full multidimensional space as required, and the trajectories were generated by classical mechanics. We argued that the classical description (in contrast to the less feasible use of quantum mechanics) was justified by the large energy released in Eq. (1.2), by the fact that equal numbers of chemical bonds are present before and after reaction (cancelling zero-point energies), and by the averaging over trajectories.

According to the polarization model, the reactants in Eq. (1.2) lie 217.506 kcal/mol higher in energy than products (all assumed unexcited and noninteracting). The principal conclusion emerging from our prior study of Reaction (1.2) is that a strong asymmetry exists in apportioning this available energy between the two product water molecules. That molecule whose oxygen originated in the hydroxide anion tends to carry away more of the reaction energy than does the other molecule formed with the hydronium oxygen. This asymmetry is striking enough to demand experimental study and verification. However it is obvious that asymmetry cannot be detected with experimentally indistinguishable product molecules.

The straightforward means of introducing the required distinguishability is isotopic substitution. Consequently we have expanded our dynamical study to include the following isotopic variants of Reaction (1.2):

$$H_3O^+ + OD^- \rightarrow H_2O + HDO \ ; \tag{1.3}$$

$$D_3O^+ + OH^- \rightarrow D_2O + HDO \ ; \tag{1.4}$$

$$D_3O^+ + OD^- \rightarrow D_2O + D_2O \ . \tag{1.5}$$

In all cases it has been supposed that the oxygen is the common isotope $O^{16}$. Only cases (1.3) and (1.4) have direct experimental significance, but in this paper we compare results for all four cases to reveal inherent influences of isotopic substitution.

It should be noted at the outset that the polarization model is manifestly an ionic picture of molecules and chemical bonding. Therefore no provision exists for molecules to fragment into neutral radicals, i.e., H and OH for water. We believe this represents a relatively unimportant channel in the present study.

Section II outlines the dynamical conditions under which the reactive collisions have been studied. Section III discusses some details of the trajectories generated, specifically which hydrogenic particle is transferred. Section IV contains our results on energy distribution between product molecules. We conclude the paper in Sec. V with discussion of and predictions for some related neutralization reactions.

## II. DYNAMICAL CONDITIONS

We have followed the same basic procedure used earlier, basing our calculations on the "PM6" version of the polarization model (see Appendix in Ref. 3). For each of the four isotopic reaction variants, Eqs. (1.2)–(1.5), 100 trajectories were generated and used to calculate properties reported below. The 100 for Reaction (1.2) were independent of those generated in our previous study, so intercomparison of the two sets of results for this case helps to gauge statistical reliability of the procedure.

To initiate each trajectory, the reactant ions in their most stable structures were placed first in the standard configuration shown in Fig. 1. This standard configuration defines a Cartesian coordinate system with the $z$

 0021-9606/82/084028-09$02.10 

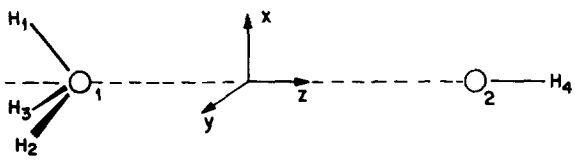


(a) STANDARD CONFIGURATION

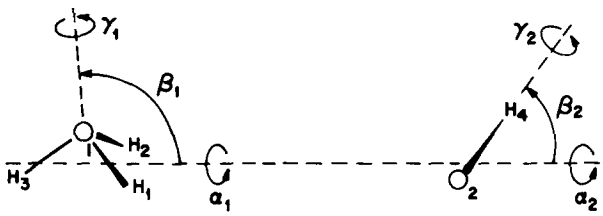


(b) RANDOMLY ROTATED REACTANTS

FIG. 1. Initial configurations for generation of the reactive collisions. The centroids of the reactant ions are placed approximately 20 Å apart along the $z$ axis, with overall center of mass at $z=0$. Random orientations are then applied to both ions (Euler angles $\alpha_1,\beta_1,\gamma_1$ for hydronium; $\alpha_2,\beta_2,\gamma_2$ for hydroxide). In this diagram $H_i$ can be either isotope H or D.

axis collinear with the symmetry axes of the ions. The ions are placed so that in the case for which all hydrogens are the light isotopic species H the reactant centroids are 20 Å apart; the overall center of mass in this case is used to define the coordinate origin. The standard configuration for the other isotope choices are the same, though the reactant ion centroids will then be slightly more than 20 Å apart on the $z$ axis. The distance between oxygens is 19.894 Å in the standard configuration.

Next, Euler angles are generated for random rotations of the reactant ions about their respective centroids. Figure 1 shows that the $z$ axis serves as polar axis for the first Euler angle ($\alpha_1$ for hydronium, $\alpha_2$ for hydroxide) in the triad of Euler angles describing the rotation of each ion. In order to minimize statistical uncertainty we chose to employ the same set of rotation angles $(\alpha_1,\beta_1,\gamma_1,\alpha_2,\beta_2,\gamma_2)$ for initiation of *four* trajectories, one for each of the isotopic variants (1.2)–(1.5).

The dynamics investigated here correspond to reactants that infinitely far in the past were infinitely separated and had no translational, rotational, or vibrational excitation. By falling toward one another under their mutual electrostatic attraction the ions have been supposed to gain only translational motion by the time that they reach the approximately 20 Å separation at which the detailed trajectory calculation begins. Consequently equal velocities $v_1$ (in the $+z$ direction) are assigned at this position to each of the four particles comprising the hydronium cation, while velocities $v_2$ (in the $-z$ direction) are assigned to the two particles comprising the hydroxide anion. The magnitudes of $v_1$ and $v_2$ depend on which isotopes are present, and they are assigned so that (a) the overall center of mass remains stationary, and (b) the initial kinetic energy at this computational starting point is attributable to the change $\Delta\Phi$ in potential energy experienced by the reactants as they are brought inward from infinity to the given configuration. Clearly $\Delta\Phi$ will depend somewhat on the random orientations applied to the ions, but it is invariably negative on account of the dominating influence of charge–charge attraction.

Several options exist for monitoring the course of reactive collisions. We have found that a convenient and revealing way is to observe time variation of the quantities $S_O$ and $S_H$, the rms distances respectively of the oxygens and the hydrogens from the fixed system center of mass.

As discussed below there is some variation in the times necessary for ions to collide, react, and eject the pair of resulting water molecules. Consequently we have applied a termination criterion at which numerical integration of the dynamical equations is halted that specifically accounts for such variation. During the course of the integration procedure the time was identified at which $S_O(t)$ had risen to twice its initial value $S_O(0)$. This could only occur if the neutralization reaction had indeed been completed, and places the two product water molecules approximately 40 Å apart while receding rapidly from one another. The trajectory was then followed for 1 ps longer, and over this last 1 ps interval various kinetic energy averages were evaluated for the essentially noninteracting products. At the final configuration, energies and angular momenta for the individual molecules (the conserved quantities for the asymptotic regime) were tabulated.

## III. COLLISION DYNAMICS RESULTS

Figures 2–5 show how $S_O(t)$ varies during reaction for one of the trajectory quadruplets (#53 in each set of 100). They correspond respectively to Eqs. (1.2)–(1.5), i.e., to increasing total mass. We stress once again that rotation angles for ions were identical for these four trajectories. We present these four to illustrate features encountered repeatedly throughout the entire study. The corresponding $S_H(t)$ curves are similar, except for somewhat more obvious vibrational fine structure.

Figures 2 and 3 both involve transfer of light hydrogen ions $H^+$. Here the reaction is "simple," with $S_O(t)$ exhibiting a single minimum. The ions achieve this minimum separation at roughly 0.3 ps, $H^+$ transfer immediately occurs, and the large energy released drives the products rapidly away. By contrast Figs. 4 and 5 show double minima for the two cases involving transfer of the heavier $D^+$. Evidently in these latter two cases the transfer was *not* effected on first encounter, but required rebound and second collision between still-ionic fragments. Such rebound collisions were encountered before in our prior study of Reaction (1.2), though rarely. It appears that deuteration of the cation markedly increases the chance for these rebounds, or relatively long-lived complexes, to occur. We find the following frequencies of such events:

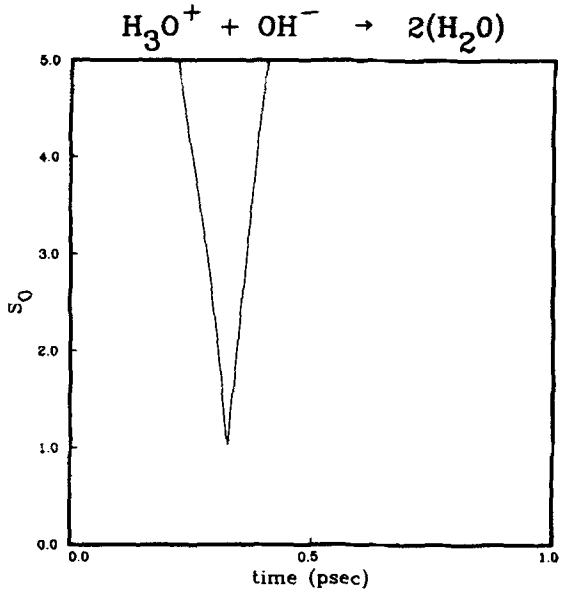


FIG. 2. Time variation of $S_0$ for Reaction (1.2), trajectory #53.

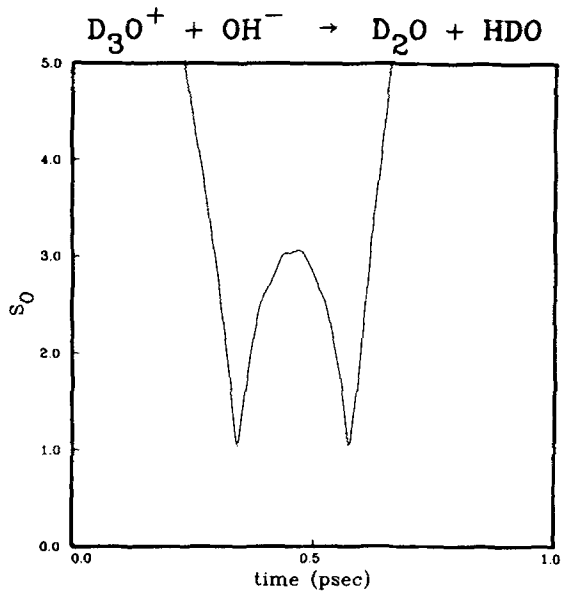


FIG. 4. Time variation of $S_0$ for Reaction (1.4), trajectory #53.

Eq. (1.2): 1/100 ,
Eq. (1.3): 3/100 ,
Eq. (1.4): 20/100 , (3.1)
Eq. (1.5): 18/100 .

Our earlier study[3] revealed a strong correlation between Euler angle $\alpha_1$ describing the hydronium orientation at the initial 20 Å separation and the identity of the particle transferred. Figures 6–9 show plots for the four cases of the transfer probabilities versus $\alpha_1$ for the three hydrogen ions. Figure 6 confirms our earlier observation, showing reasonably clear separation in $\alpha_1$ for the three distinct transfer possibilities when the pure-light-isotope case (1.2) is involved. Figure 7 shows that this separation pattern is nearly preserved when only the anion is deuterated. But when the cation is deuterated (Figs. 8 and 9) the distributions spread out much more and overlap along the $\alpha_1$ axis. Two classes of results thus arise, distinguishable by the mass of the particle being transferred. This correlates in turn with the rebound fractions (3.1). An obvious explanation is that infall from 20 Å twists the hydronium relatively little ($\alpha_1$ controls which of the three hydrogens initially points toward the recipient hydroxide), but that rebounds tend to reorient strongly.

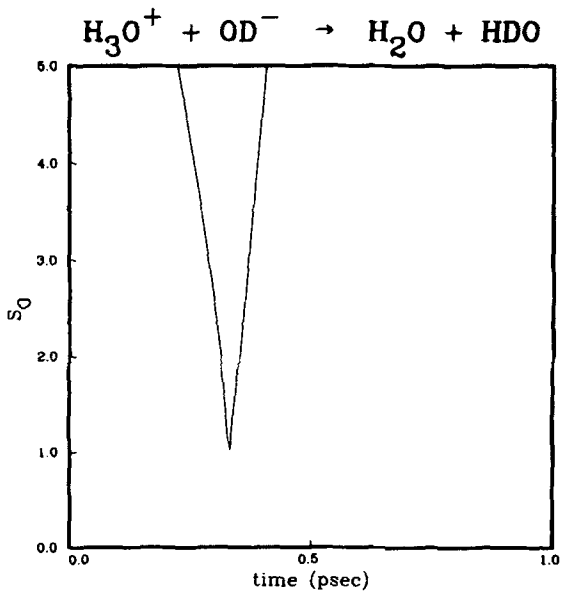


FIG. 3. Time variation of $S_0$ for Reaction (1.3), trajectory #53.

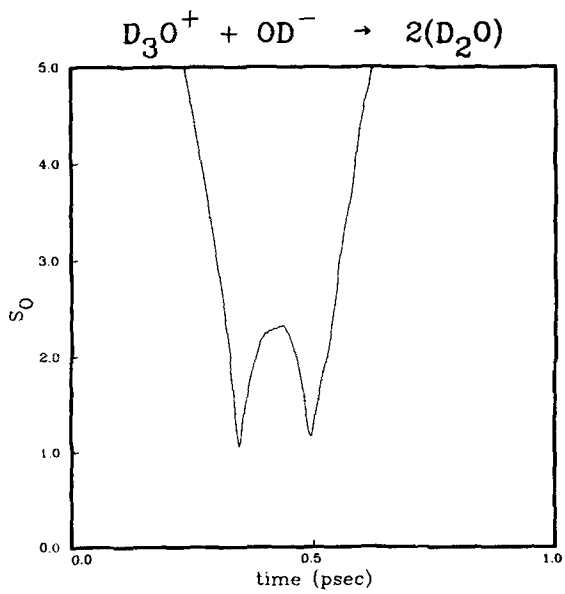


FIG. 5. Time variation of $S_0$ for Reaction (1.5), trajectory #53.

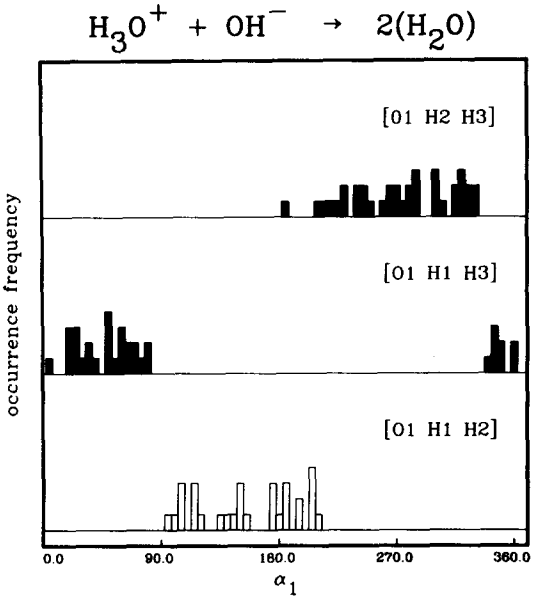


FIG. 6. Occurrence frequencies for specific hydrogen transfer vs initial Euler angle $\alpha_1$. These results refer to the pure-light-hydrogen case, Reaction (1.2). The brackets for the three plots indicate which particles (as named in Fig. 1) comprise the product water molecule originating in the hydroniums (black, shaded, and white histograms indicate $H_1$, $H_2$, and $H_3$ transfers, respectively).

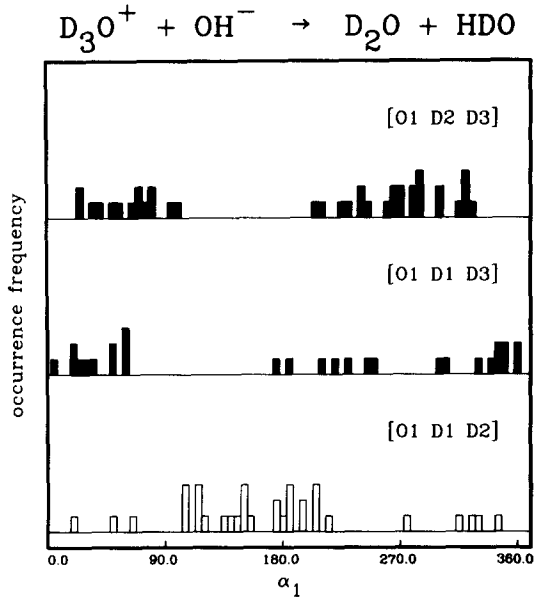


FIG. 8. Occurrence frequencies for specific hydrogen transfer vs Euler angle $\alpha_1$, for Reaction (1.4).

Figure 10 presents the entire set of "reaction channel" identifications for the 400 trajectories, indicating schematically which numbered hydrogen transfers. In each horizontal row the results shown correspond to increasing overall mass from left to right, i.e., Reaction (1.2) is at the left, (1.3) is next, followed by (1.4), and the fully deuterated (1.5) is at the right. It is interesting to note the number of changes in hydrogen label that occur across each of the three mass increases. In passing from Reaction (1.2) to Reaction (1.3) only three changes occur. Between Reactions (1.3) and (1.4) however 33 changes occur. Between Reactions (1.4) and (1.5) there are 18 changes. Once again we see that replacement of transferring light hydrogen by more massive deuterium tends to complicate the outcome of the reaction dynamics.

Distributions of product scattering angles relative to the fixed $z$ axis in Fig. 1 have been calculated. These distributions are isotropically distributed around the $z$ axis of course, but can vary in polar angle. Figures

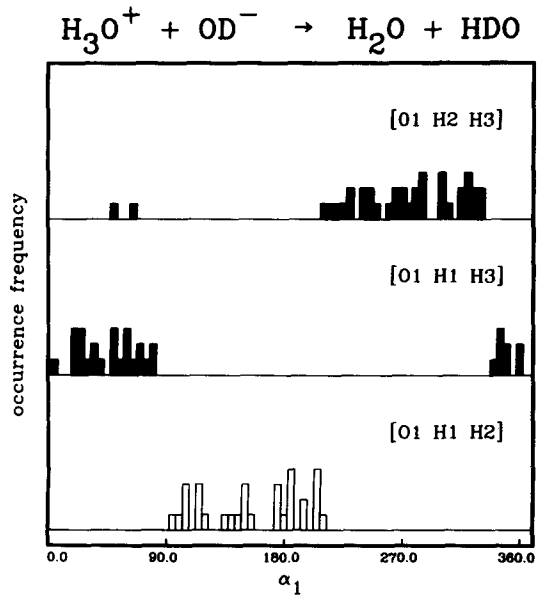


FIG. 7. Occurrence frequencies for specific hydrogen transfer vs Euler angle $\alpha_1$, for Reaction (1.3).

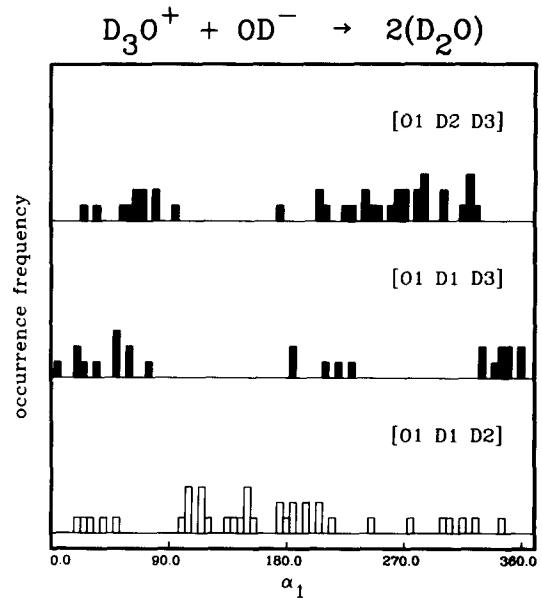


FIG. 9. Occurrence frequencies for specific hydrogen transfer vs Euler angle $\alpha_1$, for Reaction (1.5).

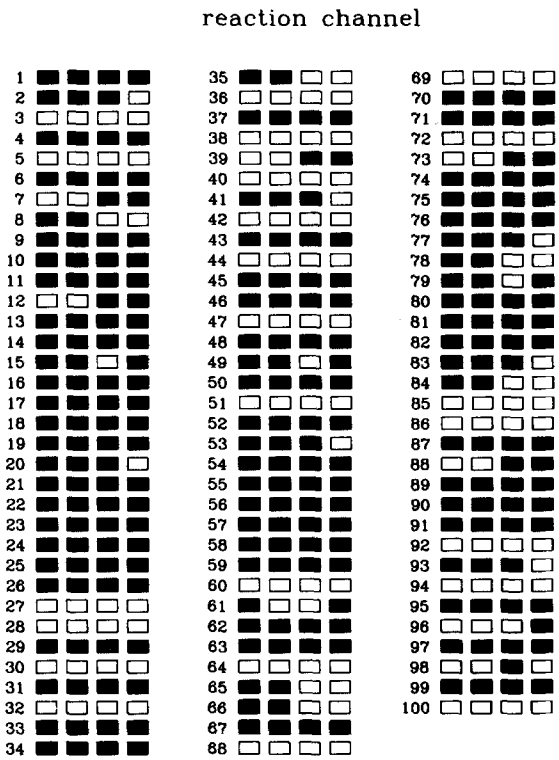


FIG. 10. Identity of transferred hydrogen for all 400 trajectories. Overall mass increases from left to right, i.e., the reactions appear in the order: (1.2), (1.3), (1.4), and (1.5). Black rectangles indicate that $H_1$ has transferred, while shaded rectangles represent $H_2$ transfers and white rectangles denote $H_3$ transfers (see Fig. 1).

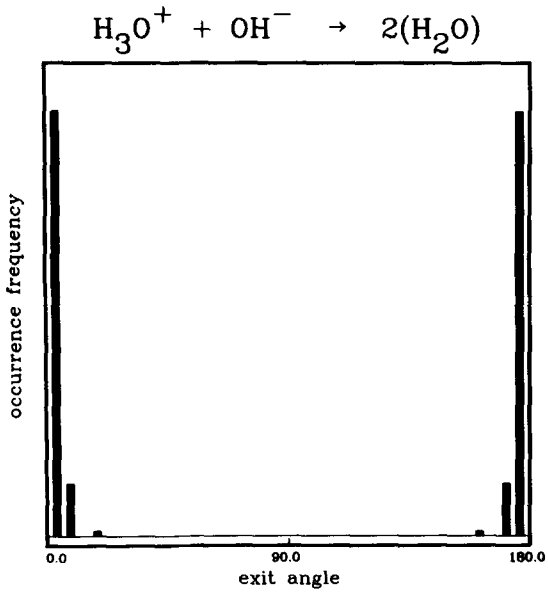


FIG. 11. Distribution of product directions (relative to the $z$ axis in Fig. 1) for Reaction (1.2). Black and shaded bars refer respectively to hydroxide and hydronium waters.

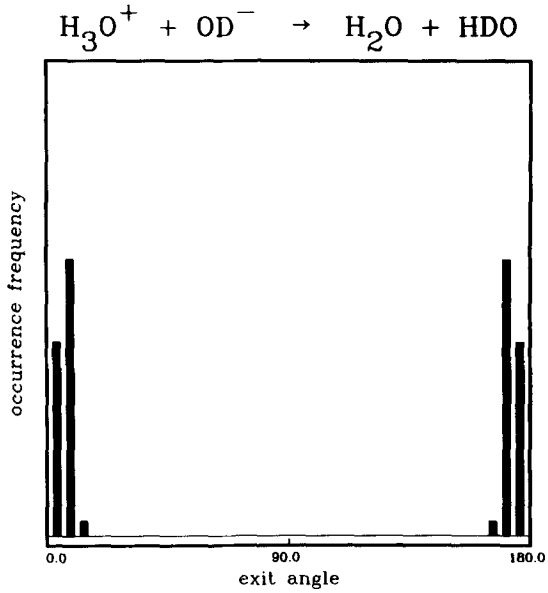


FIG. 12. Distribution of product directions for Reaction (1.3).

11–14 show the distributions of angles (bin width 5°) for the emerging neutrals, obtained from the molecular centroids at the end of each computed trajectory. The distributions are different from one another, but once again the isotopic mass of the transferring hydrogen ion exerts the dominant influence. For $H^+$ transfer [Figs. 11 and 12, Reactions (1.2) and (1.3)] the products emerge strongly collimated in forward and backward directions; the collisions are usually "simple" and linear. By contrast $D^+$ transfer [Figs. 13 and 14, Reactions (1.4) and (1.5)] has a greater angular spread of emerging neutrals. Evidently the time elapsed during the frequent rebounds is enough to permit rotation of the reaction complex, so the hot neutrals are then kicked away off of the $z$ axis.

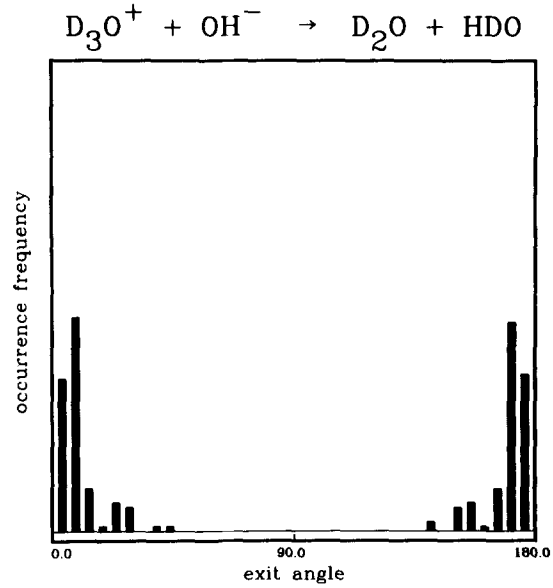


FIG. 13. Distribution of product directions for Reaction (1.4).

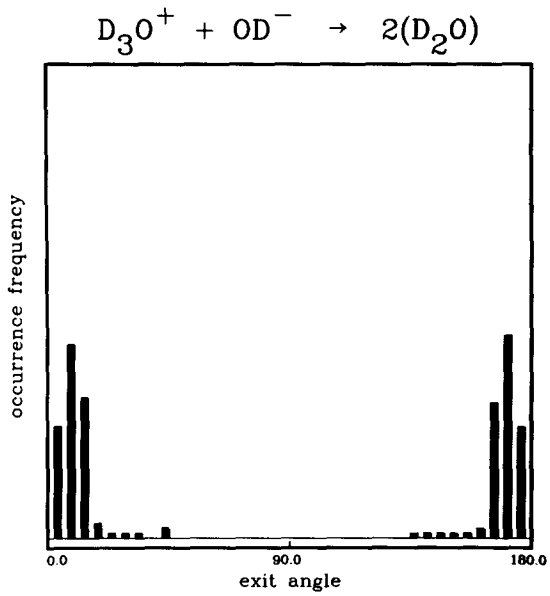


FIG. 14. Distribution of product directions for Reaction (1.5).

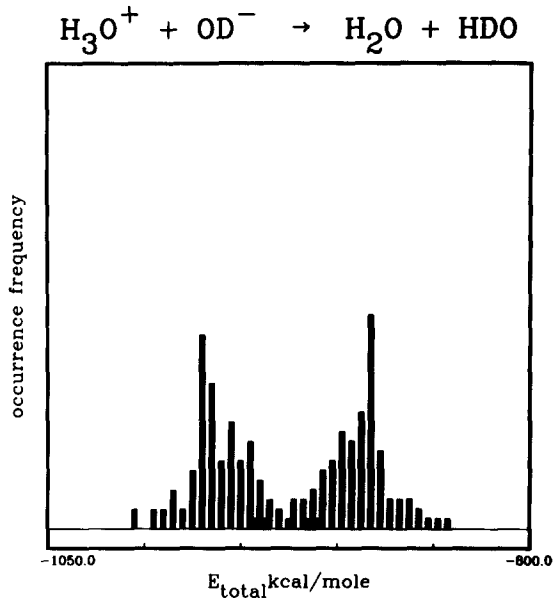


FIG. 16. Distributions of energies for the water molecules produced by Reaction (1.3).

## IV. ENERGY DISTRIBUTIONS

The energy of a stationary water molecule at its mechanical equilibrium geometry is −1032.924 kcal/mol according to the polarization model. The excess energy that product water molecules bear after the reactive collision resides partly in their center-of-mass translational motion, and partly in the internal motion of coupled rotation and vibration.

Figure 15 presents the distributions of final energies found for the two water molecules created by Reaction (1.2). It is very clear from the figure that those molecules whose oxygen originated in the hydroxide anion (black bars) tend to be more highly excited than those whose oxygen originated in the hydronium (shaded bars). This accords with the findings reported in Ref. 3. The respective average energies of excitation were found to be 136.2 and 81.3 kcal/mol.

Figure 16 shows the corresponding product energies for the deuterated-anion case, Reaction (1.3), where as before the light isotopic species $H^+$ is transferred. Once again the distributions are rather well separated, with the water molecules (now HDO) formed from the anion tending to be the more strongly excited. The average

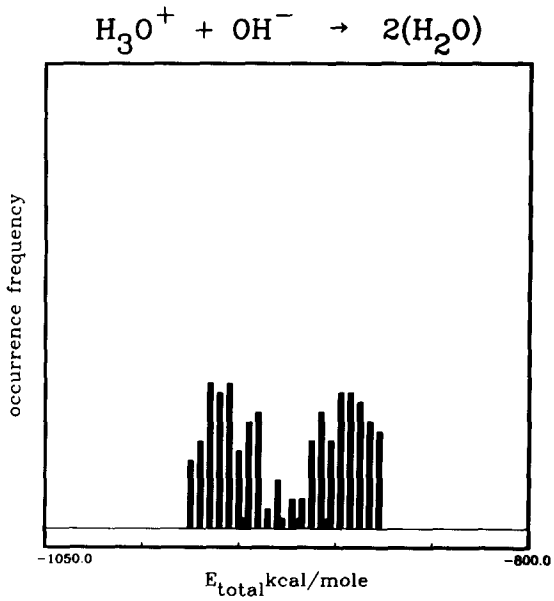


FIG. 15. Distributions of energies for the water molecules produced by Reaction (1.2). Shaded bars refer to water molecules originating as hydronium, black bars refer to water molecules originating as hydroxide.

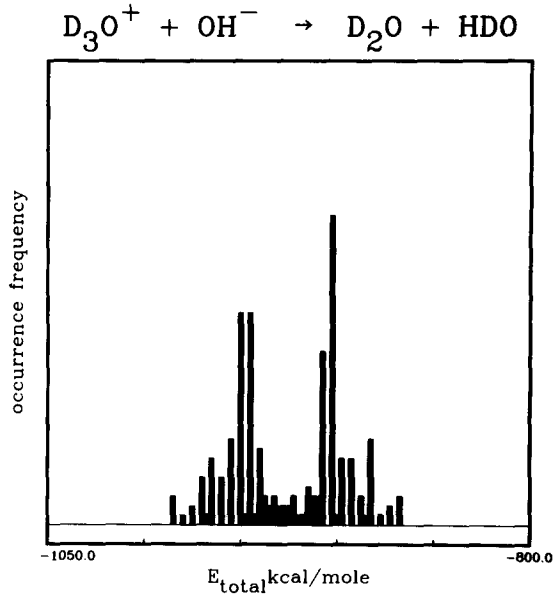


FIG. 17. Distributions of energies for the water molecules produced by Reaction (1.4).

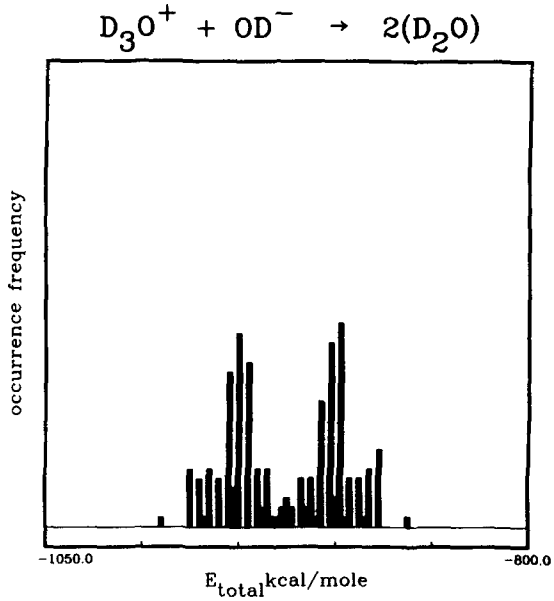


FIG. 18. Distributions of energies for the water molecules produced by Reaction (1.5).

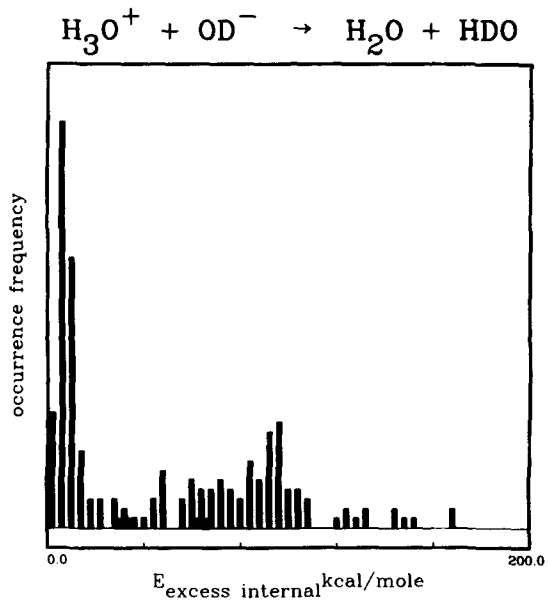


FIG. 20. Distributions of excess internal energy for the water molecules produced by Reaction (1.3).

excitation energies are now 143.1 kcal/mol (for HDO) and 74.4 kcal/mol (for $H_2O$). Comparison of Figs. 15 and 16 seems to suggest that the single anion deuteration has produced a shape change in the distributions, with the latter case exhibiting greater breadth.

Figure 17 presents the energy distributions for Reaction (1.4), where now $D^+$ transfers. Once more the water originating in the anion tends to have the larger energy, but the distributions overlap more than before. The average excitation energies are found to be 129.9 kcal/mol (for HDO) and 87.6 kcal/mol (for $D_2O$).

The distributions shown in Fig. 18 refer to Reaction (1.5) for the fully deuterated species. These resemble those in Fig. 17 more than those in Figs. 15 or 16, again illustrating the primary importance of the mass of the transferred hydrogenic particle. The average excitation energies for this last case are 130.1 kcal/mol ($D_2O$ from $OD^-$) and 87.4 kcal/mol ($D_2O$ from $D_3O^+$).

The distributions of excitation energies shown in Figs. 15–18 contain contributions both from translational kinetic energy and from internal motions. Since these are separable it is desirable to isolate the contribution of the latter in its own distributions. Figures 19–22 do

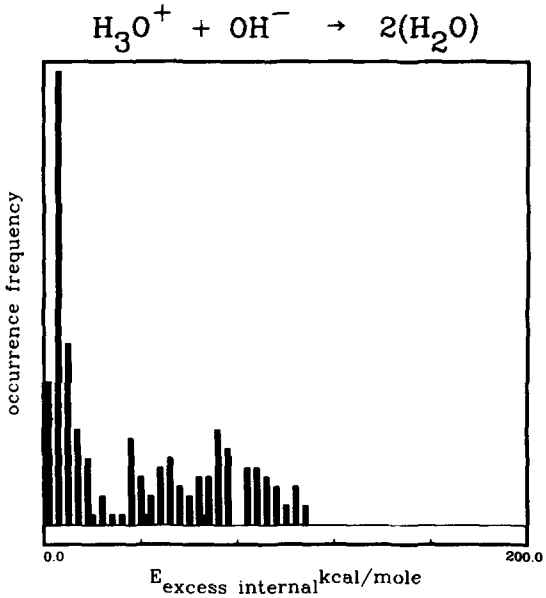


FIG. 19. Distributions of excess internal energy for the water molecules produced by Reaction (1.2). Black and shaded bars refer respectively to hydroxide and hydronium water.

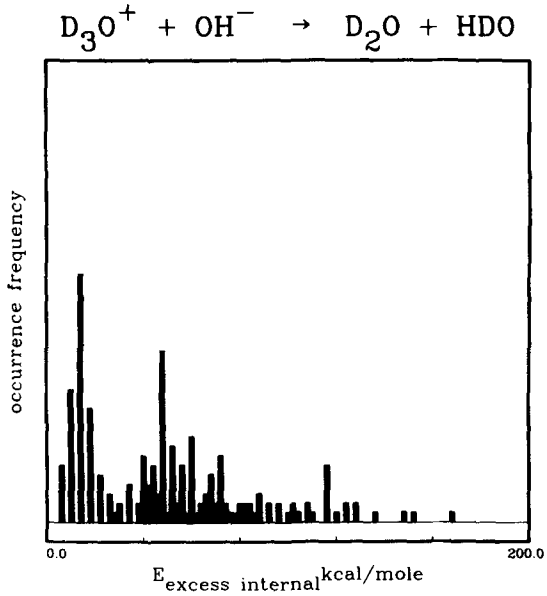


FIG. 21. Distributions of excess internal energy for the water molecules produced by Reaction (1.4).

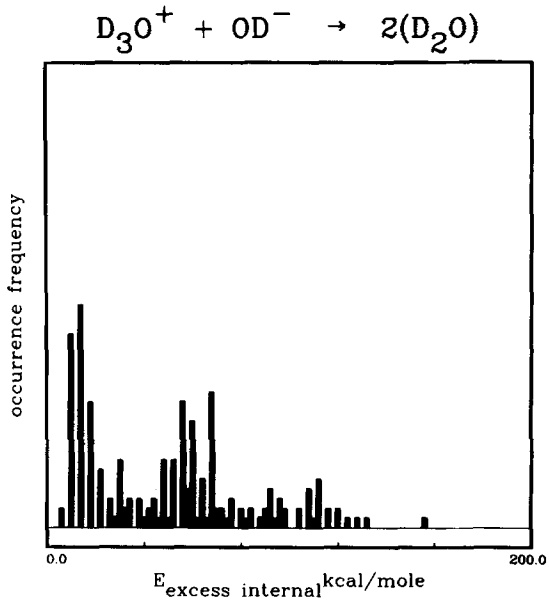


FIG. 22. Distributions of excess energy for the water molecules produced by Reaction (1.5).

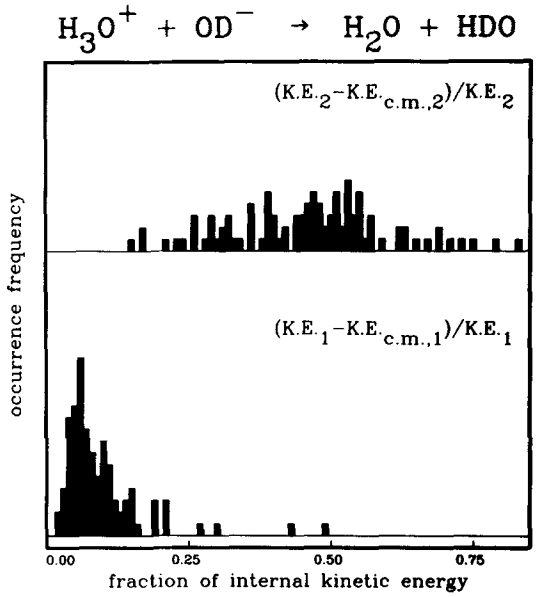


FIG. 24. Distributions of time-averaged kinetic energy of internal motion for the water molecules produced by Reaction (1.3).

just that by presenting for Reactions (1.2)–(1.5), in order, the excess internal energies found in product water molecules. The same pattern continues to emerge. These internal degrees of freedom tend on average to be much more highly excited for the "anion" water than for the "cation" water. Furthermore the change from $H^+$ transfer (Figs. 19 and 20) to $D^+$ transfer (Figs. 21 and 22) again causes the distributions to overlap more.

Yet another view of the difference in extent of internal excitation for the product molecules emerges from time-averaged kinetic energies. The kinetic energy associated with internal degrees of freedom is not a conserved quantity, but its time average exists. We have used the last ps of each trajectory to compute these averages; this should be a satisfactory interval considering the frequencies involved. Figures 23–26 display the respective distributions for Reactions (1.2)–(1.5). The previous themes continue to be illustrated.

Our prior publication[3] reported excess kinetic energy distributions of internal motion for the light-isotope-reactant case (1.2). That Fig. 23 so closely resembles this earlier result reinforces the contention that 100 trajectories is a sufficiently large set to reveal principal features of the neutralization reaction.

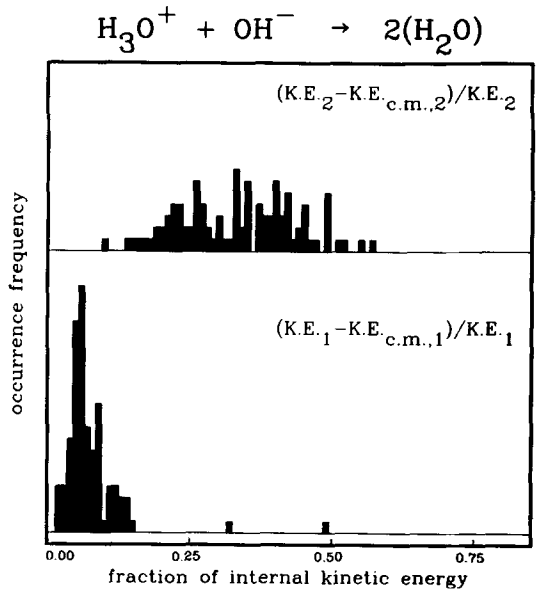


FIG. 23. Distributions of time-averaged kinetic energy of internal motion for the water molecules produced by Reaction (1.2). Black and shaded bars refer respectively to hydroxide and hydronium waters.

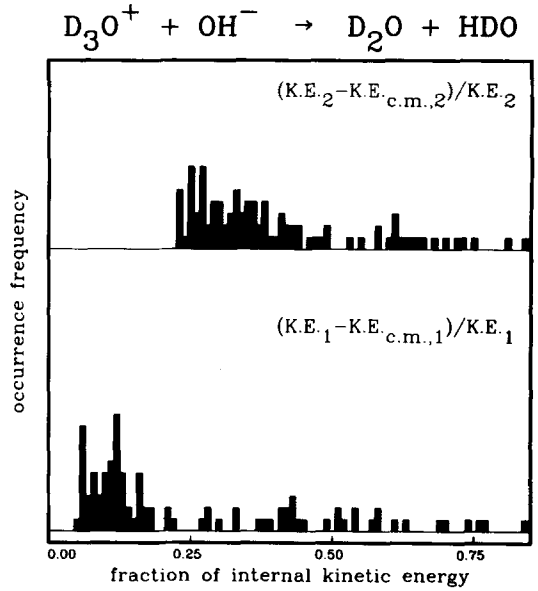


FIG. 25. Distributions of time-averaged kinetic energy of internal motion for the water molecules produced by Reaction (1.4).

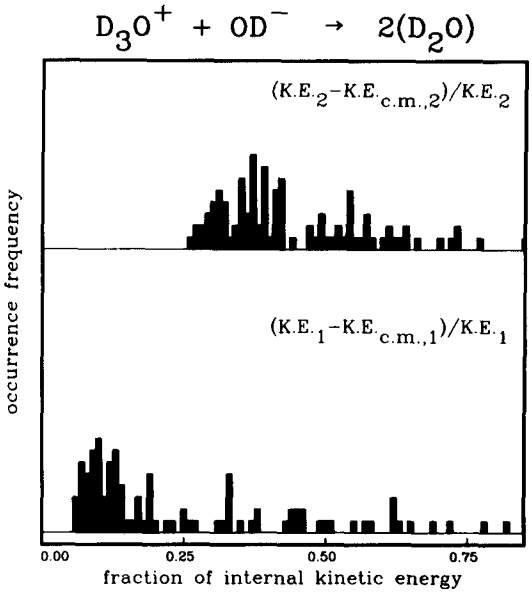


FIG. 26. Distributions of time-averaged kinetic energy of internal motion for the water molecules produced by Reaction (1.5).

## V. DISCUSSION

The calculations reported in this paper reaffirm the phenomenon reported in Ref. 1, namely that in the hydronium–hydroxide neutralization reaction the energy released tends to concentrate on the hydrogen-ion recipient molecule. Although this phenomenon persists under partial or complete deuteration significant isotope effects are present, the most important determinant of which is the mass of the transferred particle. These results have obvious implications for the experimentally interesting cases represented by Reactions (1.3) and (1.4).

It is natural to speculate at this stage that the energy asymmetry between proton (or deuteron) donor and acceptor fragments may have wide applicability. For example, the reaction which generalizes those considered above,

$$H_{2n+1}O_n^+ + H_{2n-1}O_n^- \rightarrow 2n(H_2O) \qquad (5.1)$$

may exhibit analogous behavior for $n > 1$. In particular the energy distribution functions for those water molecules originating in the anionic reactant might exhibit higher degrees of excitation compared to those originating in the cationic reactant. This speculation is susceptible to study by straightforward extension of the calculations reported here.

It would also be worthwhile to pursue study of analogous proton transfer reactions such as the following:

$$H_2F^+ + F^- \rightarrow 2HF\ ; \qquad (5.2)$$

$$NH_4^+ + NH_2^- \rightarrow 2NH_3\ . \qquad (5.3)$$

Polarization model potentials have in fact already been determined both for the hydrogen fluoride system[4] and for the ammonia system.[5] The dynamical studies (including isotopic effects) should be comparable in difficulty to that reported in this paper.

Finally we remark that the polarization model and the dynamics it generates are also applicable to proton transfer reactions of the type

$$HA^+ + B \rightarrow A + HB^+\ , \qquad (5.4)$$

where B is a better Lewis base than A, i.e., B has a greater proton affinity than A. An example would be $H_2O$ and $NH_3$ for A and B, respectively. Much less energy is released in this class of transfer reactions compared to those involving neutralization. Consequently if excitation energy asymmetry is present it may be less dramatic. However Reactions (5.4) are experimentally attractive in that easily detectable ions are produced rather than just neutral molecules as in neutralization. In any case the polarization model is also capable of probing these cases as well, and we expect in the near future to undertake numerical studies of selected examples.

[1]F. H. Stillinger and C. W. David, J. Chem. Phys. **69**, 1473 (1978).
[2]F. H. Stillinger and T. A. Weber, Chem. Phys. Lett. **79**, 259 (1981).
[3]T. A. Weber and F. H. Stillinger, J. Phys. Chem. (to be published).
[4]F. H. Stillinger, Int. J. Quantum Chem. **14**, 649 (1978).
[5]P. J. Turner and C. W. David, J. Chem. Phys. **74**, 512 (1981).